Development 133, 3629-3639 (2006) doi:10.1242/dev.02543

# Connexin 43-mediated modulation of polarized cell movement and the directional migration of cardiac neural crest cells

**Xin Xu, Richard Francis, Chih Jen Wei, Kaari L. Linask and Cecilia W. Lo***

Connexin 43 knockout (Cx43α1KO) mice have conotruncal heart defects that are associated with a reduction in the abundance of cardiac neural crest cells (CNCs) targeted to the heart. In this study, we show CNCs can respond to changing fibronectin matrix density by adjusting their migratory behavior, with directionality increasing and speed decreasing with increasing fibronectin density. However, compared with wild-type CNCs, Cx43α1KO CNCs show reduced directionality and speed, while CNCs overexpressing Cx43α1 from the CMV43 transgenic mice show increased directionality and speed. Altered integrin signaling was indicated by changes in the distribution of vinculin containing focal contacts, and altered temporal response of Cx43α1KO and CMV43 CNCs to β1 integrin function blocking antibody treatment. High resolution motion analysis showed Cx43α1KO CNCs have increased cell protrusive activity accompanied by the loss of polarized cell movement. They exhibited an unusual polygonal arrangement of actin stress fibers that indicated a profound change in cytoskeletal organization. Semaphorin 3A, a chemorepellent known to inhibit integrin activation, was found to inhibit CNC motility, but in the Cx43α1KO and CMV43 CNCs, cell processes failed to retract with semaphorin 3A treatment. Immunohistochemical and biochemical analyses suggested close interactions between Cx43α1, vinculin and other actin-binding proteins. However, dye coupling analysis showed no correlation between gap junction communication level and fibronectin plating density. Overall, these findings indicate Cx43α1 may have a novel function in mediating crosstalk with cell signaling pathways that regulate polarized cell movement essential for the directional migration of CNCs.

**KEY WORDS: Connexin 43, Neural crest cell, Focal contact, Actin cytoskeleton, Cell motility**

## INTRODUCTION

Neural crest cells are ectomesenchymal cells derived by epithelial-mesenchyme cell transformation from the dorsal neural tube. They disperse throughout the embryo, generating all of the cells in the peripheral nervous system, craniofacial connective tissue and bone, pigmented cells in the skin, and cells in the adrenal medulla. Neural crest cells also migrate to the heart and play an essential role in cardiovascular development (Kirby and Waldo, 1995). This is mediated by a subpopulation of neural crest cells derived from the post-otic hindbrain neural fold to somite level 3, referred to as the cardiac neural crest cells (CNCs). Ablation studies as well as various mutant animal models have shown that perturbation or deletion of CNCs can lead to cardiovascular defects involving outflow tract septation anomalies, such as persistent truncus arteriosus as well as various aortic arch anomalies (Kirby and Waldo, 1995). In addition, CNCs play an essential role in patterning of coronary arteries. Thus appropriate targeting of CNCs to the heart is of crucial importance for survival of the animal.

Neural crest cells from different axial levels of the neural tube employ different migratory pathways, with cardiac CNCs shown to migrate along a circumpharyngeal pathway to reach the aortic arches and heart (Kirby et al., 1983; Lumsden et al., 1991). The deployment of CNCs to the heart has been shown to be modulated by interactions mediated by connexin 43 (Cx43α1) gap junctions. Gap junctions are specialized cell junctions encoded by connexin proteins that contain membrane channels that mediate the movement of ions and small molecules between cells. CNCs express Cx43α1, and are functionally well-coupled through gap junction channels (Lo et al., 1999). Cx43α1 knockout (Cx43α1KO) mice die at birth with conotruncal heart malformations, outflow obstructions and coronary anomalies (Huang et al., 1998b; Li et al., 2002; Reaume et al., 1995). Studies carried out using the Cx43α1KO mice and transgenic mice overexpressing Cx43α1 or expressing a dominant-negative form of Cx43α1 showed CNC motility is dependent on the precise level of Cx43α1 function. Thus, loss or dominant-negative inhibition of Cx43α1 inhibited neural crest cell migration, resulting in fewer CNCs targeted to the outflow tract (Huang et al., 1998a; Sullivan and Lo, 1995). By contrast, in CMV43 transgenic mice overexpressing Cx43α1, neural crest cell migration was enhanced, and this was associated with an excess of CNCs in the outflow tract (Huang et al., 1998a). Motion analysis using timelapse videomicroscopy showed Cx43α1-deficient CNCs have reduced directionality (Xu et al., 2001). Although these studies provide compelling evidence of a role for Cx43α1 in modulating cell motility, the underlying mechanism is unknown.

In this study, we examined whether the altered motile behavior of CNCs from the Cx43α1KO and CMV43 transgenic mice may involve perturbation in integrin signaling. Integrins are heterodimeric receptors that, upon matrix binding, cluster to form focal contacts that link the extracellular matrix to the actin cytoskeleton. The dynamic assembly and disassembly of focal contacts play an essential role in polarized cell movement and directional cell migration. Neural crest cells are known to express multiple integrins (Delannet et al., 1994; Monier-Gavelle and Duband, 1997). Perturbation studies have shown integrins play an essential role in modulating the migratory behavior of neural crest cells (Alfandari et al., 2003; Strachan and Condic, 2003). Our studies suggest altered integrin

Laboratory of Developmental Biology, National Heart, Lung and Blood Institute, National Institutes of Health, Bethesda, MD 20850, USA.

*Author for correspondence (e-mail: loc@nhlbi.nih.gov)

**Accepted 20 July 2006**

signaling in CNCs from the Cx43α1KO and CMV43 CNCs. Changes in motile behavior was associated with altered regulation of polarized cell movement. This was accompanied by changes in the distribution of focal contacts, and also marked changes in the organization of the actin cytoskeleton in the Cx43α1KO CNCs. However, we found no correlation between the level of gap junction communication and changes in motile cell behavior. Given these observations, we considered the possibility that Cx43α1 may modulate cell motile behavior through crosstalk with proteins that dynamically regulate the actin cytoskeleton. Consistent with this, we observed colocalization of Cx43α1 with many actin-binding proteins.

## MATERIALS AND METHODS

### Mouse breeding and genotyping

Cx43α1KO embryos were generated from interbreeding heterozygous Cx43α1KO animals, and CMV43 transgenic mice were bred to obtain homozygous and heterozygous CMV43 embryos (Huang et al., 1998a). PCR genotyping was carried using DNA obtained from yolk sac tissue. The protocol used for genotyping the Cx43α1KO mice were modified as previously reported (Reaume et al., 1995). Primer pairs for detecting the CMV43 transgene are: CMV-F1, 5′-TGTTCCCATAGTAACGCCAATAGG-3′; CMV-B7, 5′-ATATAGACCTCCCACCGTACACGC-3′. Homozygous CMV43 embryos were identified by quantitative real time PCR using primer pairs: DHFR-F3, 5′-CGAAACTGACAGCACATCGTAGG-3′; DHFR-B4, 5′-CACTCGTGAATGCGTTATCGTTC-3′; GAPDH-F9, 5′-ATGTTCCAGTATGACTCCACTCACG-3′; GAPDH-B6, 5′-GAAGACACCAGTAGACTCCACGACA-3′.

### Neural tube explant cultures

Embryos used for neural tube explant cultures were harvested at E8.5 day as described previously (Moiseiwitsch and Lauder, 1995). The hindbrain neural folds were collagenase/dispase (Roche, Indianapolis, IN) treated, and the dorsal ridge of the neuroepithelium spanning the postotic region of the hindbrain neural fold was surgically removed from the surrounding tissue and cultured on plates coated with human plasma fibronectin (Life Technologies or Sigma) in Dulbecco's modified Eagle's medium (DMEM) with high glucose and 10% fetal bovine serum (FBS).

### Cell adhesion assay

CNCs were isolated from 46-hour explant cultures and were resuspended in 0.1 ml of DMEM containing 10% FBS. Cell suspensions were plated in five or more replicates and allowed to attach for 20 minutes at 37°C in 96-well plates coated with 15 μg/ml fibronectin and blocked with 1% BSA for 1 hour at room temperature. Cell attachment was measured by assaying for ATP levels of adherent cells divided by total cells seeded. ATP was detected using ATPlite Kit from Perkin Elmer (Wellesley, MA).

### Motion analysis

Neural tube explants were cultured in phosphate buffered L-15 medium (Sigma) containing 10% FBS and placed on a 37°C heated stage of the Leica DMIRE2 inverted microscope. Timelapse images were captured using an Orca-ER camera. For monitoring the directionality (net path length/total path length) and speed of cell locomotion, images were captured using a 10× objective every 10 minutes over a 20 hour interval, while cell protrusive activity was monitored using a 63× objective with images captured every 5 minutes over a 2-hour interval or every minute over 20 minutes with or without semaphorin 3a (Sema3a). Sema3a/FC chimeric protein was obtained from R&D (Minneapolis, MN), and used at a final concentration of 500 ng/ml in culture medium. Quantitative motion analysis was carried out using Dynamic Image Analysis Software (Solltech, Oakdale, IA). For this analysis, the outline of individual cells located at or near the migration front of the emerging explant were traced frame by frame. Using these tracings, the DIAS software calculated the speed and directionality of cell movement by tracking the change in the position of the centroid of the cell at each time point. Using DIAS, the protrusive activity of the cell was quantitatively assessed by measuring the amount of new cell area formed versus cell area lost. This is expressed as percent area expansion or contraction and is referred to as 'positive' versus 'negative' flow. In addition, using these same cell tracings, roundness was calculated, which is defined as $100 \times 4\pi$ (area/perimeter$^2$) (Stites et al., 1998), which is a measure of how efficiently a given amount of perimeter encloses area: a circle has the largest area for any given perimeter with a roundness of 100%. Thus, the greater the number of cell protrusions, the lower the roundness. All of the data obtained from these quantitative assessments were evaluated by ANOVA using Statview (SAS Institute, Cary, NC).

### Antibodies and reagents

Antibodies used included: rabbit polyclonal 18-A8 recognizing cytoplasmic tail of Cx43α1 (1:1500; kindly supplied by Dr Elliot Hertzberg, Albert Einstein College of Medicine), mouse monoclonal anti-vinculin antibody (Sigma; 1:500), rat monoclonal anti-β1 integrin antibody (Chemicon; 1:100), mouse monoclonal anti-ezrin antibody (Transduction Lab; 1:100), mouse monoclonal anti-α-actinin (Sigma; 1:500), mouse monoclonal anti-IQGAP-1 (Upstate Technology, 1:100), rhodamine-phalloidin (Sigma; 1:500) and Drebrin (Stressgen Biotechnology, 1:100). The fluorescence-conjugated secondary antibodies were obtained from Jackson ImmunoResearch Laboratories. Goat anti-rat β1 integrin function blocking antibody was provided by Dr Borg's laboratory (Gullberg et al., 1989). Cytochalasin D was purchased from Sigma.

### Immunohistochemistry

Immunohistochemistry was carried out by epifluorescence microscopy using a 40× or 63× oil objective on a Leica DMRE microscope. All images were captured using a Hamamatsu Micromax or Orca-ER CCD camera. Images were obtained as *z*-stacks composed of 0.2 μm optical slices, and deconvolved by nearest neighbor or iterative deconvolution algorithms using Openlab deconvolution software (Improvision, Lexington, MA). To quantitate focal contacts, we measured vinculin immunofluorescence using images captured at the plane of the cell-substrate interface. The measurements were made by tracing the outlines of individual cells and measuring the intensities and area of immunofluorescence per cell to yield mean intensity and mean area of vinculin immunostaining. To evaluate the organization of the actin cytoskeleton, we visualized actin filaments with rhodamine phalloidin and counted the number of stress fiber bundles seen as dense actin filament arrays (loosely arrayed actin filaments were not counted), and we also measured the length of actin stress fiber bundles. To assess the alignment directionality of stress fiber bundles, we measured the angle between stress fiber bundles. This was carried out by delineating a line to demarcate the orientation of each stress fiber bundles in a cell, and measuring the angle between the stress fiber bundles. In cells with more than

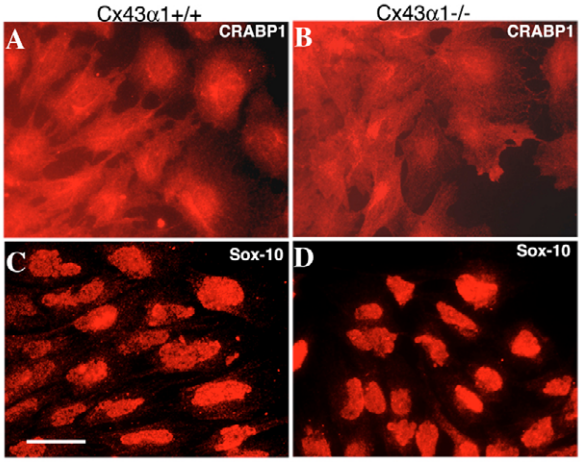


**Fig. 1. CNC explants express neural crest markers.** Immunostaining show expression of Crabp1 (**A**,**B**) and Sox10 (**C**,**D**), two neural crest markers, in CNCs emerging from postotic hindbrain neural tube explants derived from wild-type (A,C) and Cx43α1KO (B,D) mouse embryos. Scale bar: 50 μm.

two stress fiber bundles, we measured the angle between the adjacent stress fiber bundles. In some experiments, CNCs were treated with cytochalasin D (1 μM) for 1 hour, then washed three times with PBS, followed by incubation for 1 hour in medium without cytochalasin D, and then fixed and stained with rhodamine phalloidin to examine the organization of the actin cytoskeleton.

### Immunoprecipitation and western immunoblotting

CNCs in explant cultures were cell surface biotinylated using 1 mM NHS-LC Biotin (Pierce Chemical, IL) for 15 minutes followed by wash with buffer containing 50 mM $NH_4Cl$ to remove non-incorporated biotin. The cells were then solubilized with 400 μl cold lysis buffer (50 mM Tris, pH 7.5 containing 0.15 M NaCl, 1% Triton X-100, 1 mM $CaCl_2$, 1 mM $MgCl_2$ and 2 mM PMSF). After centrifugation at 12,000 ***g*** for 10 minutes at 4°C, supernatant was removed and incubated with 2.5 μl goat anti-integrin antibody (5 mg/ml) overnight at 4°C followed by adding 50 μl protein G-agarose (1:1 in PBS) for 2 hours at 4°C (rocking). After extensive washing (five times in 50 mM Tris pH 7.5, 0.15 M NaCl, 0.1% Tween-20, twice in same buffer containing 0.5 M NaCl, and once in 0.05 M Tris pH 6.8), the immunoprecipitates were separated by 10% SDS-PAGE and blotted onto PVDF membrane, followed by immunodetection using streptavidin HRP and enzyme-linked chemiluminescence detection system (Amersham Biosciences). The co-immunoprecipitation experiment was carried out as described previously (Wei et al., 2005).

### Quantitative analysis of gap junction communication

To assess gap junction communication in CNCs, dye-coupling experiments were carried out with microelectrode impalements and iontophoretic injections of carboxyfluorescein. Neural tube explant cultures were plated in L-15 medium and placed on 37°C heated Leica DMLFSA microscope stage. Dye injections were carried out using microelectrodes back filled with 2% carboxyfluorescein. After intracellular microelectrode impalement, iontophoretic dye injection was carried out for 2 minutes and then the microelectrode was removed. After a further 2 minutes for additional cell-to-cell spread of the dye, dark-field image and DIC images were captured for the quantitative assessment of the extent of dye spread. Using the DIC image, the outlines of individual cells were traced and merged with the dark-field image. Using this merged image, the number of dye filled cells versus non-dye filled cells were counted, and the percentage of dye-filled primary neighbors (directly adjacent to injected cell), secondary neighbors (directly adjacent to primary neighbors) and tertiary neighbors (directly adjacent to secondary neighbors) was calculated.

## RESULTS

### Neural crest explants express neural crest specific markers

Postotic hindbrain neural folds were dissected from E8.5 mouse embryos and explanted in culture. Cells emerging from this axial level of the neural tube give rise to a subpopulation of neural crest cells that migrate to the heart, i.e the CNCs (Waldo et al., 1999). To confirm the identity of these outgrowth as neural crest cells, we immunostained these explants with antibodies to retinoic acid binding protein 1 (Crabp1) (Lee et al., 1995) or Sox10 (De Bellard et al., 2002; Southard-Smith et al., 1998). Both proteins were found to be expressed at high levels in cells emerging from these explant cultures, with Sox10 showing nuclear localization as expected (Fig. 1). We found no difference in the pattern of immunostaining in wild-type versus Cx43α1KO explants (Fig. 1), and similar results were also obtained for CMV43 CNC explants (not shown). Immunostaining of mouse fibroblast cells using these same antibodies resulted in only nonspecific background staining (not shown).

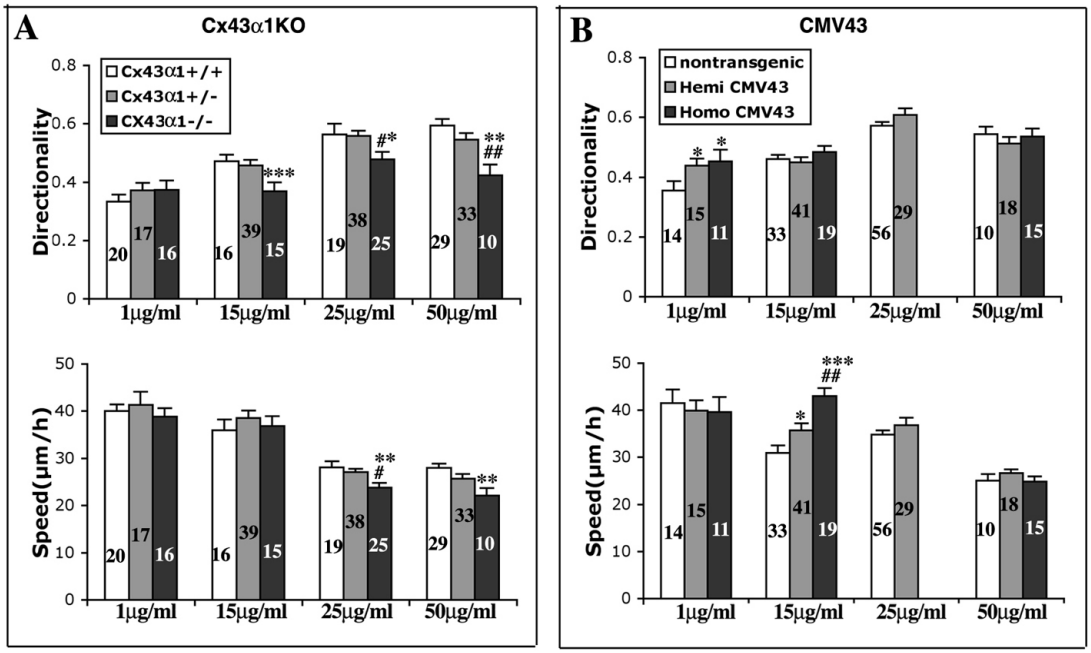


**Fig. 2. Cx43α1 modulation of neural crest cell motility on fibronectin.** The speed and directionality of cell locomotion was quantitatively assessed using time lapse images of CNCs explants from Cx43α1KO and CMV43 embryos plated on different fibronectin coating densities. Images were captured every 10 minutes over a 20-hour interval. As fibronectin density increased, wild-type and nontransgenic control CNCs (clear bars) show increased directionality, but decreased speed of cell locomotion (**A**,**B**). However, Cx43α1KO cells failed to achieve high directionality, while their speed of cell locomotion decreased more rapidly (A). By contrast, CMV43 neural crest cells exhibited higher directionality and higher speed of cell locomotion at 1 and 15 μg/ml fibronectin, respectively (B). Numbers in bars indicate the total number of cells analyzed. Error bars indicate the s.e.m. **P*<0.05; ***P*<0.01; ****P*<0.001, compared with wild type. $^{\#}P$<0.05; $^{\#\#}P$<0.01; $^{\#\#\#}P$<0.001, compared with hemi- or heterozygotes.

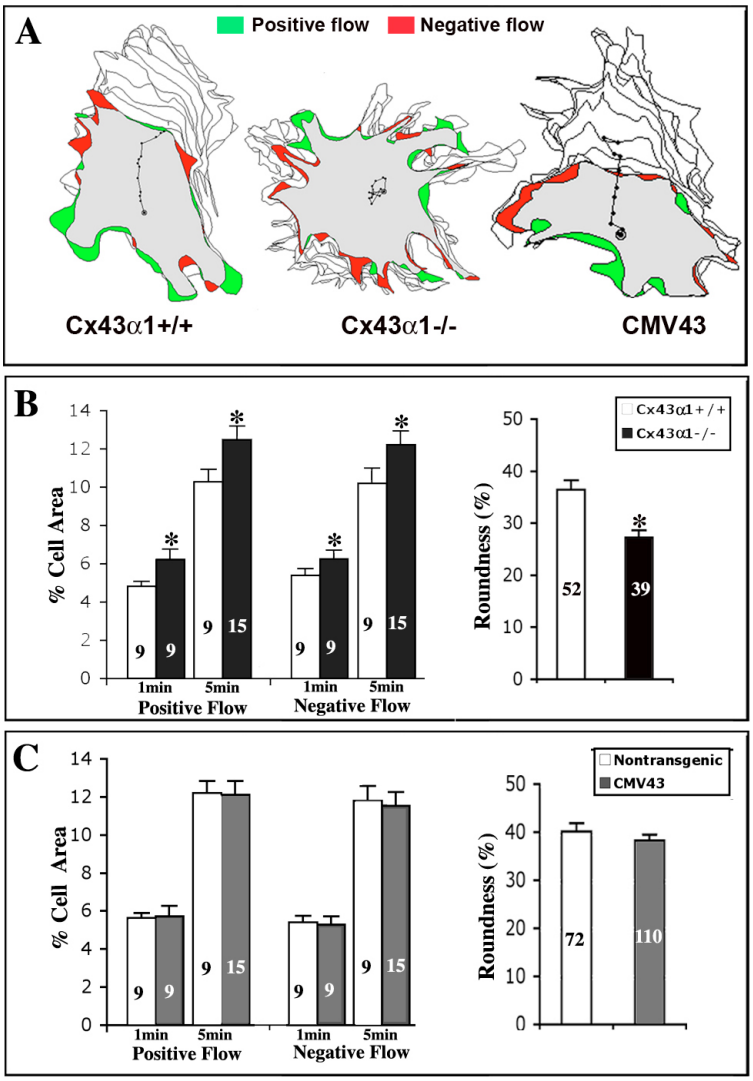


**Fig. 3. Cx43α1 modulation of cell protrusive activity.** (**A**) Time lapse image stacks obtained from individual Cx43α1$^{+/+}$, Cx43α1$^{-/-}$ and CMV43 CNCs captured at 5-minute intervals. Area of expansion or positive flow is indicated in red; area of contraction or negative flow is indicated in green. The image on top represents the cell at the last two frames, with underlying cell outlines corresponding to the preceding 10 timelapse imaging frames. (**B**,**C**) Cell protrusive activity in Cx43α1KO (B) and CMV43 (C) CNCs was quantitatively assessed by measuring positive (green) and negative (red) cytoplasmic flow. Roundness was also analyzed, which provided a measure of cell shape and was calculated using formula 100% × 4π (area/perimeter$^2$), with the maximal roundness being 100% for a circle. The Cx43α1KO cells showed increased positive and negative flows, together with decreased roundness (B), while no change in positive/negative flow or roundness was seen for the CMV43 CNCs (C). *$P$<0.05 when compared with Cx43α1+/+ or nontransgenic controls. The numbers of cells analyzed are indicated in the bars.

## Cardiac neural crest cell adhesion and migration on fibronectin

CNCs were assayed for adhesion to fibronectin by harvesting the neural crest outgrowths, plating the resuspended CNCs onto dishes coated with 15 μg/ml fibronectin and quantitating the percentage of cells bound to the substratum 20 minutes after plating. Cx43α1KO CNCs showed a 25% reduction in adhesion compared with wild-type cells ($P$<0.05), while CMV43 CNCs showed no change compare with their nontransgenic control. Using timelapse videomicroscopy, we further assessed motile behavior of CNCs with different expression level of Cx43α1 on different fibronectin density using dishes coated with 1, 15, 25 or 50 μg/ml fibronectin. Analysis of the migratory paths of individual neural crest cells revealed increased directionality, but decreased speed of cell locomotion as fibronectin density increased (Fig. 2A,B). In contrast to wild-type cells, homozygous Cx43α1KO CNCs failed to achieve high directionality, even at high fibronectin density, while their speed decreased more rapidly with increasing fibronectin density (Fig. 2A). However, CMV43 CNCs showed enhanced cell motility, exhibiting high directionality even at low fibronectin density (1 μg/ml), while maintaining high speed even as fibronectin density was elevated (15 μg/ml) (Fig. 2B).

To further assess the modulation of directional cell movement by Cx43α1, we quantitatively assessed cell protrusive activity by monitoring the extension and retraction of cell processes using time lapse imaging, with images captured at either 1 or 5 minute intervals over a period of 2 hours (see Movies 1 and 2 in the supplementary material). Using these time lapse images, the outlines of individual cells were manually traced and the percent cell area expansion versus contraction between two consecutive time frames were used to calculate ‘positive flow’ (shown in green in Fig. 3A) versus ‘negative flow’ (shown in red in Fig. 3A). Cx43α1KO CNCs showed an increase in both positive and negative flow when compared with CNCs from wild-type littermate controls (Fig. 3B), while CMV43 CNCs were indistinguishable from CNCs from nontransgenic littermate controls (Fig. 3C). We also measured the roundness of the cells using the formula 100% × 4π (area/perimeter$^2$), such that a circle would have maximal roundness at 100% (Stites et al., 1998). Consistent with increased protrusive activity, the Cx43α1KO CNCs showed a decrease in roundness, while no change in roundness was observed for the CMV43 CNCs (Fig. 3C). Wild-type and CMV43 CNCs showed a distinct polarized distribution of green positive flow at the leading edge and red negative flow at the trailing edge of the cell, as would be expected for directional cell movement (Fig.

3A,C). However in the Cx43α1KO CNCs, the areas of positive and negative flow were distributed nearly symmetrically around the entire cell periphery (see red and green areas in Fig. 3A). The lack of polarity in cell protrusive activity is consistent with the decrease in the directionality of cell movement in Cx43α1KO CNCs (Fig. 2).

## Cx43α1 perturbation alters the distribution of β1-integrin and focal contacts

Using immunohistochemistry, we examined expression of β1 integrin in CNCs, as β1 integrin is known to play an important role in mediating fibronectin binding. Double immunostaining was carried out with β1 integrin and vinculin antibodies. Wild-type CNCs showed discrete β1 integrin membrane localization largely towards the cell periphery, at regions overlapping with vinculin containing focal adhesions (Fig. 4A). In Cx43α1KO CNCs, we observed a reduction in β1 integrin and vinculin immunostaining (Fig. 4B), while in CMV43 CNCs, β1 integrin and vinculin immunostaining remained abundant (Fig. 4C). To investigate if cell surface expression of β1 integrin might be altered by Cx43α1 perturbation, western immunoblotting analysis was carried out. CNCs in explants were cell-surface biotinylated, then cell extracts were made and immunoprecipitated with a β1 integrin antibody, followed by western immunoblotting with streptavidin. A predominant band at 120 kDa was obtained, the molecular weight expected for β1 integrin (Fig. 4D). Quantitative analysis showed no difference in the abundance of this 120 kDa band in the wild-type versus CMV43 CNCs (Fig. 4D). Comparable analysis of β1 integrin expression in Cx43α1KO CNCs was not feasible, given the limited abundance of KO CNCs.

As vinculin containing focal contacts provide the actin cytoskeletal linkages essential for matrix adhesion and cell motility, we quantitatively assessed the distribution of vinculin containing focal contacts in wild-type, Cx43α1KO and CMV43 CNCs plated on different fibronectin matrix density (1, 15 and 50 μg/ml). Compared with wild-type CNCs, Cx43α1KO CNCs exhibited a reduction in the mean area and mean intensity of vinculin immunostaining at all fibronectin coating densities (Fig. 4E). By contrast, CMV43 CNCs showed an increase in vinculin intensity, with the mean area showing a decrease at 15 μg/ml fibronectin (Fig. 4F). These findings suggest Cx43α1 deficiency versus overexpression has differing effects on the organization of focal contacts in the Cx43α1KO versus CMV43 CNCs.

## Cx43α1 modulates the actin cytoskeleton

As cell protrusive activity and the formation of focal contacts are dynamically regulated by the actin cytoskeleton, we used rhodamine-phalloidin staining to examine actin cytoskeletal organization. We observed marked differences in the actin cytoskeleton in the wild-type versus KO CNCs. Wild-type CNCs typically exhibited two major stress fiber bundles that are aligned to the long axis of the cell body (Fig. 5A), while KO CNCs showed three and on occasion four intersecting bundles that encircled the cell cortex in a polygonal arrangement (Fig. 5B). To assess these changes quantitatively in the organization of the actin cytoskeleton, we measured the number of stress fiber bundles per cell, the mean length of the actin stress fibers and the angle between stress fiber bundles. The latter provided an assessment of the alignment orientation

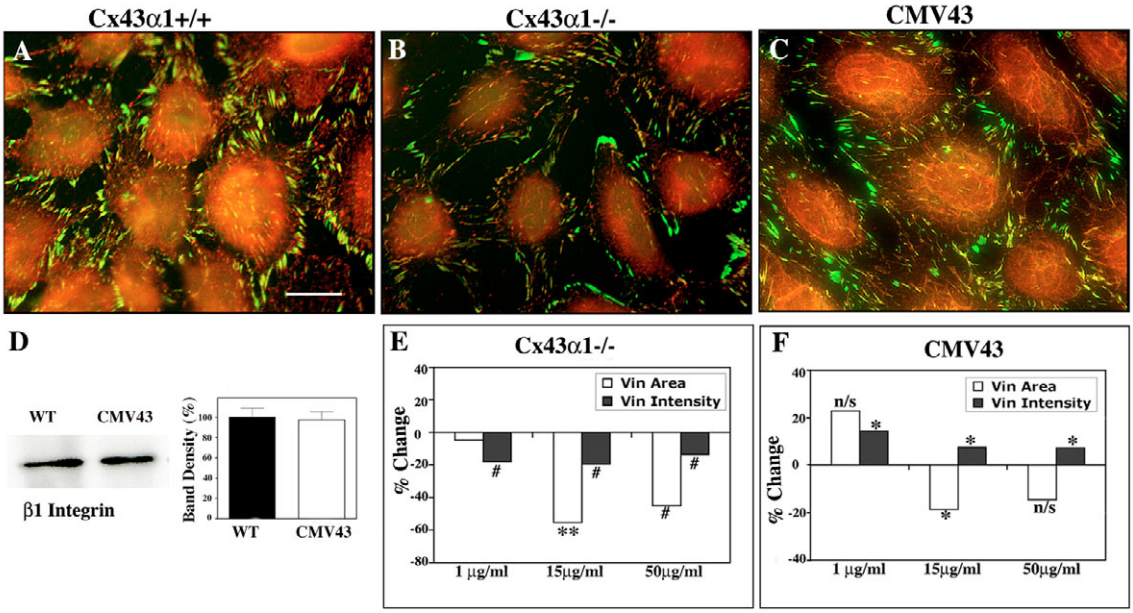


**Fig. 4. Alterations in focal adhesion contacts in Cx43α1 KO and CMV43 CNCs.** (**A-C**) CNC cells from wild-type (A), Cx43α1KO (B) and CMV43 (C) embryos were cultured on 15 μg/ml fibronectin matrix. Cells were double immunostained with antibodies against β1 integrin (red) or vinculin (green). Cx43α1KO cells show reduced β1 integrin and vinculin immunostaining (B). In CMV43 CNCs, the pattern of β1 integrin and vinculin immunofluorescence is qualitatively changed, with the intensity of vinculin immunostaining showing a noticeable increase (C). Magnification is same in all panels. Scale bar: 50 μm. (**D**) To examine if β1 integrin is expressed in CNCs, wild-type and CMV43 CNC explants were surface biotinylated, then cell extracts were made, followed by immunoprecipitation using a β1 integrin antibody and western immunoblotting using stretpavidin-peroxidase. This yielded a 120 kDa band, the size expected for β1 integrin. No difference was detected in the surface β1 integrin expression level in the CMV43 and wild-type CNCs. (**E**,**F**) The mean area and mean intensity of vinculin immunofluorescence in CNCs cultured on 1, 15 and 50 μg/ml fibronectin matrix were quantitatively assessed. Cx43α1KO cells showed decreases in vinculin area and intensity (E), while CMV43 cells showed an increase in vinculin intensity (F). **P*<0.05, ***P*<0.01; #*P*<0.0005. n/s, no significant difference, when compared with Cx43α1+/+ or nontransgenic cells.

between stress fiber bundles. Thus Cx43α1KO CNCs exhibited an alignment of 83±4°, when compared with 39±5° for wild-type CNCs. This increase in alignment angle reflects the polygonal arrangement of actin stress fibers in the KO CNCs. Cx43α1KO CNCs also exhibited significantly shorter stress fiber bundles, together with an increase in the number of stress fiber bundles per cell (Table 1). Double staining of cells with phalloidin and a vinculin antibody showed stress fiber bundles in wild-type CNCs were anchored terminally by vinculin containing focal adhesions (Fig. 5C), but stress fiber bundles in the Cx43α1KO CNCs did not always terminate in focal adhesions (see white arrowhead in Fig. 5D). Similar analysis of actin stress fibers in CMV43 CNCs showed no detectable difference when compared with their control nontransgenic CNCs (Table 1).

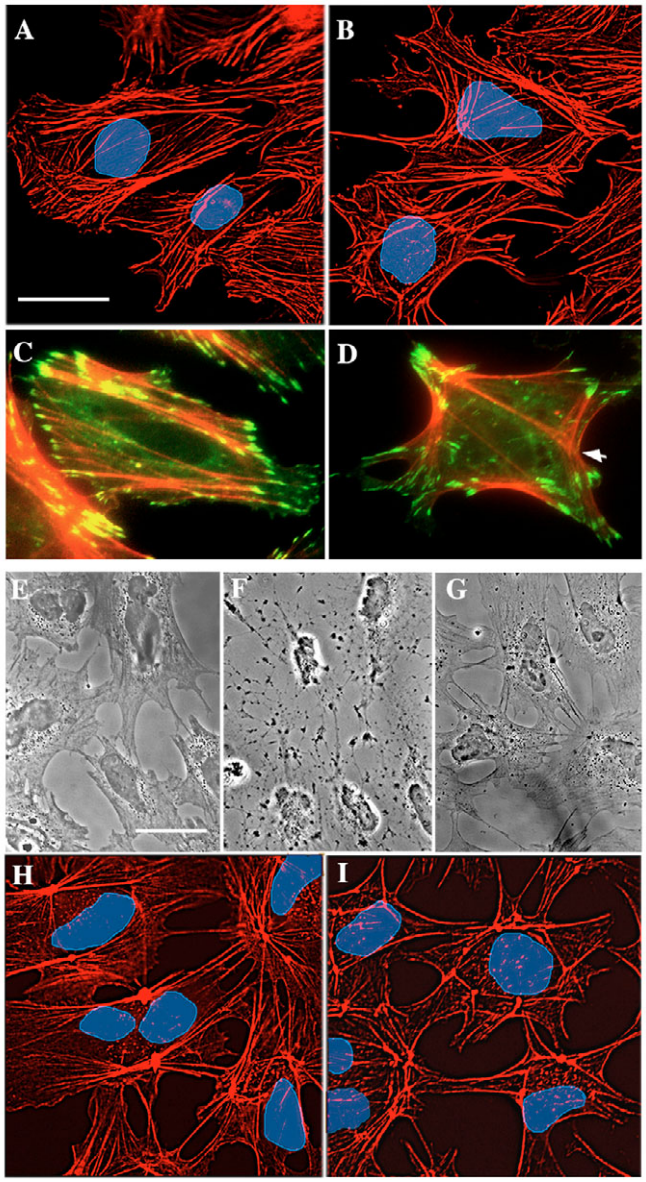


**Fig. 5. Cx43α1KO CNCs show alteration in the actin cytoskeleton.** (**A**,**B**) Rhodamine phalloidin staining showed parallel alignment of actin stress fibers in wild type CNCs (A), whereas in Cx43α1KO CNCs, stress fiber bundles were oriented in a polygonal array around the cell periphery (B). (**C**,**D**) Double immunostaining with rhodamine phalloidin (red) and vinculin (green) showed actin stress fibers typically terminated at focal adhesions in wild-type CNCs (**C**), but in Cx43α1KO cells (**D**), some actin stress fibers were not associated with focal adhesions (arrow). (**E-I**) Phase-contrast images show morphology of CNCs before (E) and after (F) cytochalasin D treatment, and 1 hour post-removal (G) of cytochalasin D. As CNCs re-establish their normal cell morphology, rhodamine phalloidin staining showed wild-type CNCs reformed parallel actin filament bundles (H), while Cx43α1KO CNCs reformed a multiangular ring of actin filaments around the cell periphery (I). Nuclei in A,B,H,I are delineated in blue using overlay of phase contrast images. Scale bars: 50 μm. Magnification is the same in A-D,H,I and in E-G.

Together these observations indicate marked changes in the organization of the actin cytoskeleton with Cx43α1KO deficiency. To further evaluate the changes in actin organization in the Cx43α1KO CNCs, we also examined the reorganization of actin filaments in CNCs recovering from cytochalasin D treatment, which causes actin filament depolymerization. As expected, CNCs treated with cytochalasin D showed a rapid and dramatic change to a round cell morphology together with the complete loss of actin filaments (Fig. 5E,F). One hour after cytochalasin removal, as cells begin to recover their normal morphology (Fig. 5G), reassembly of actin filaments can be observed by phalloidin staining (Fig. 5H,I). In such Cx43α1KO CNCs, typically four or five actin organizing centers can be seen associated with a polygonal network of forming actin filaments that encircled the cell cortex (Fig. 5I; Table 1). By contrast, wild-type CNCs typically exhibited two or three actin organizing centers with forming actin filament bundles that are aligned in parallel (Fig. 5H; Table 1). These differences in the pattern of actin filament reassembly in the wild-type versus KO CNCs are consistent with the differences seen in the organization of actin stress fibers in the untreated CNCs.

## Cx43α1 modulation of neural crest cell migration is β1-integrin dependent

To further evaluate the role of integrins in Cx43α1 modulation of CNC motility, we analyzed the effects of β1 integrin function blocking antibody on the motile behavior of CNCs. Timelapse videomicroscopy and motion analysis were carried out to quantitate the speed and directionality of cell movement at 1 hour, 2 hour and 3 hours post-antibody treatment (Fig. 6). Overall, β1 integrin function blocking antibody treatment caused a marked reduction in the speed and directionality of CNC motility, confirming a functional requirement for β1 integrin in CNC migration on fibronectin (Fig. 6). The speed of cell locomotion showed reduction in wild-type, KO and CMV43 CNCs 1 hour post-antibody treatment; by 3 hours, all three were maximally inhibited (Fig. 6B). By contrast, only wild-type CNCs showed a significant reduction in the directionality of cell locomotion after 1 hour of antibody treatment. Cx43α1KO cells showed no significant change in directionality until 2 hours post-antibody treatment, and not until 3 hours post-antibody treatment in CMV43 CNCs (Fig. 6A,B). This delay in the inhibition of directional cell movement in response to function blocking antibody treatment suggests regulation of polarized cell movement may be disturbed in the Cx43α1KO and CMV43 CNCS.

## Sema3a inhibition of cardiac neural crest cell adhesion and migration

To further evaluate Cx43α1 in modulating integrin-mediated motile cell behavior, we assessed the effects of Sema3a on CNC migration on fibronectin. Recent studies indicate semaphorins play an important role in CNC migration (Brown et al., 2001; Feiner et al., 2001), and semaphorins have been shown to inhibit cell migration

**Table 1. Quantitative assessment of actin stress fiber organization**

| Genotype | Treatment | Number of cells analyzed | Number of stress fiber bundles | Stress fiber alignment | Length |
|---|---|---|---|---|---|
| Cx43α1$^{+/+}$ | None | 29 | 2.1±0.1 | 39±5° | 32±1 μm |
| Cx43α1$^{-/-}$ | | 30 | 3.5±0.2 ($P$<0.0001) | 83±4° ($P$<0.0001) | 19±1 μm ($P$<0.0001) |
| Cx43α1$^{+/+}$ | Recovery from cytochalasin* | 15 | 2.7±0.3 | n.d. | n.d. |
| Cx43α1$^{-/-}$ | | 15 | 4.5±0.2 ($P$<0.0001) | n.d. | n.d. |
| Nontransgenic control | None | 24 | 2.2±0.1 | 32±5° | 34±2 μm |
| CMV43 | | 22 | 2.4±0.1 | 41±5° | 31±2 μm |
| Nontransgenic control | Recovery from cytochalasin* | 15 | 2.6±0.2 | n.d. | n.d. |
| CMV43 | | 18 | 2.7±0.2 | n.d. | n.d. |

n.d., not determined.
*Analysis 1 hour after cytochalasin removal.

on fibronectin through antagonizing integrin activation (Osborne et al., 2005; Pasterkamp et al., 2003; Serini et al., 2003). Timelapse videomicroscopy showed Sema3a reduced both positive and negative cytoplasmic flows in wild-type, CMV43, and Cx43α1KO CNCs (Fig. 7A,B). In wild-type CNCs, there was a concomitant increase in roundness of the cell that is consistent with the retraction of cell processes. This is reminiscent of semaphorin induced growth cone collapse in neurons (Luo et al., 1993). However, in Sema3a-treated Cx43α1KO and CMV43 CNCs, there was little change in roundness (Fig. 7A,B). This would suggest that the overall reduction in cell protrusive activity in the Cx43α1KO and CMV43 CNCs was not accompanied by the retraction of cell processes. These findings suggest a role for Cx43α1 in modulating the retraction of cell processes.

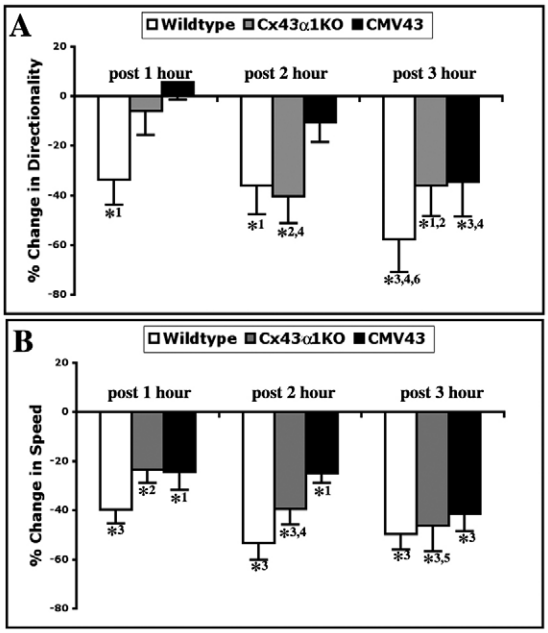


**Fig. 6. Inhibition of CNC migration by β1 integrin function blocking antibody.** The motile behavior of CNC cells treated with β1 integrin function blocking antibody was monitored by time lapse imaging and motion analysis, with images captured every 10 minutes. The change in directionality and speed of cell locomotion was compared with untreated cells and plotted as percent change in directionality (**A**) or speed (**B**). The wild-type CNCs show a reduction in speed and directionality within 1 hour of antibody treatment. The Cx43α1 KO and CMV43 CNCs showed a delayed response to the inhibitory effects of the antibody treatment. Error bars indicate s.e.m. *1 $P$<0.05, *2 $P$<0.01, *3 $P$<0.001 when compared with pre-antibody treatment; *4 $P$<0.05, *5 $P$<0.01 when compared with 1 hour of antibody treatment; *6 $P$<0.05 when compared with 2 hours of antibody treatment. Number of cells analyzed: 16, wild type; 19, Cx43α1KO; 20, CMV43.

## Cx43α1 interactions with vinculin and actin-binding proteins

To examine if Cx43α1 might interact with integrin or vinculin, we carried out double immunostaining to examine the subcellular distribution of Cx43α1 with β1 integrin or vinculin. Cx43α1 and β1 integrin did not colocalize (data not shown), while colocalization was observed for Cx43α1 and vinculin (Fig. 8A-C). This was largely at regions of cell-cell contact (white arrowheads in Fig. 8C). To further investigate the nature of this interaction biochemically, we

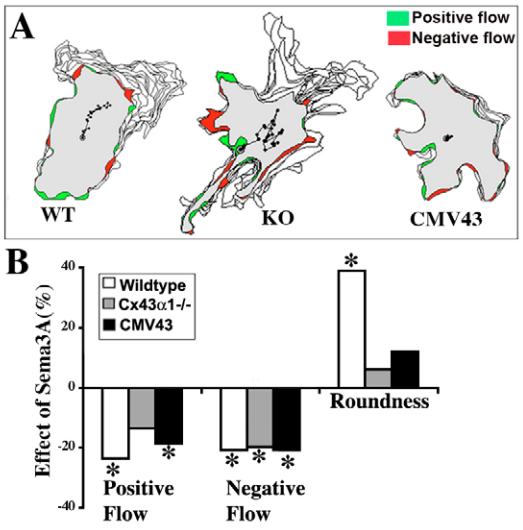


**Fig. 7. Cx43α1 perturbation alters the response of CNCs to Sema3a.** (**A**) Timelapse images of Cx43α1$^{+/+}$, Cx43α1$^{-/-}$ and CMV43 CNCs treated with Sema3a. Images were captured at 1-minute intervals over 20 minutes, with area of expansion indicated by green (positive flow) and area of contraction indicated in red (negative flow). The image on top represents the cell at the last time frame, with underlying cell outlines corresponding to preceding timelapse frames. (**B**) Positive and negative flows were decreased in wild-type, Cx43α1KO and CMV43 CNCs after Sema3a treatment, but the cell roundness was increased only in the wild-type CNCs (B). Error bars indicate s.e.m. *$P$<0.05, when compared with cells without Sema3A of same genotype.

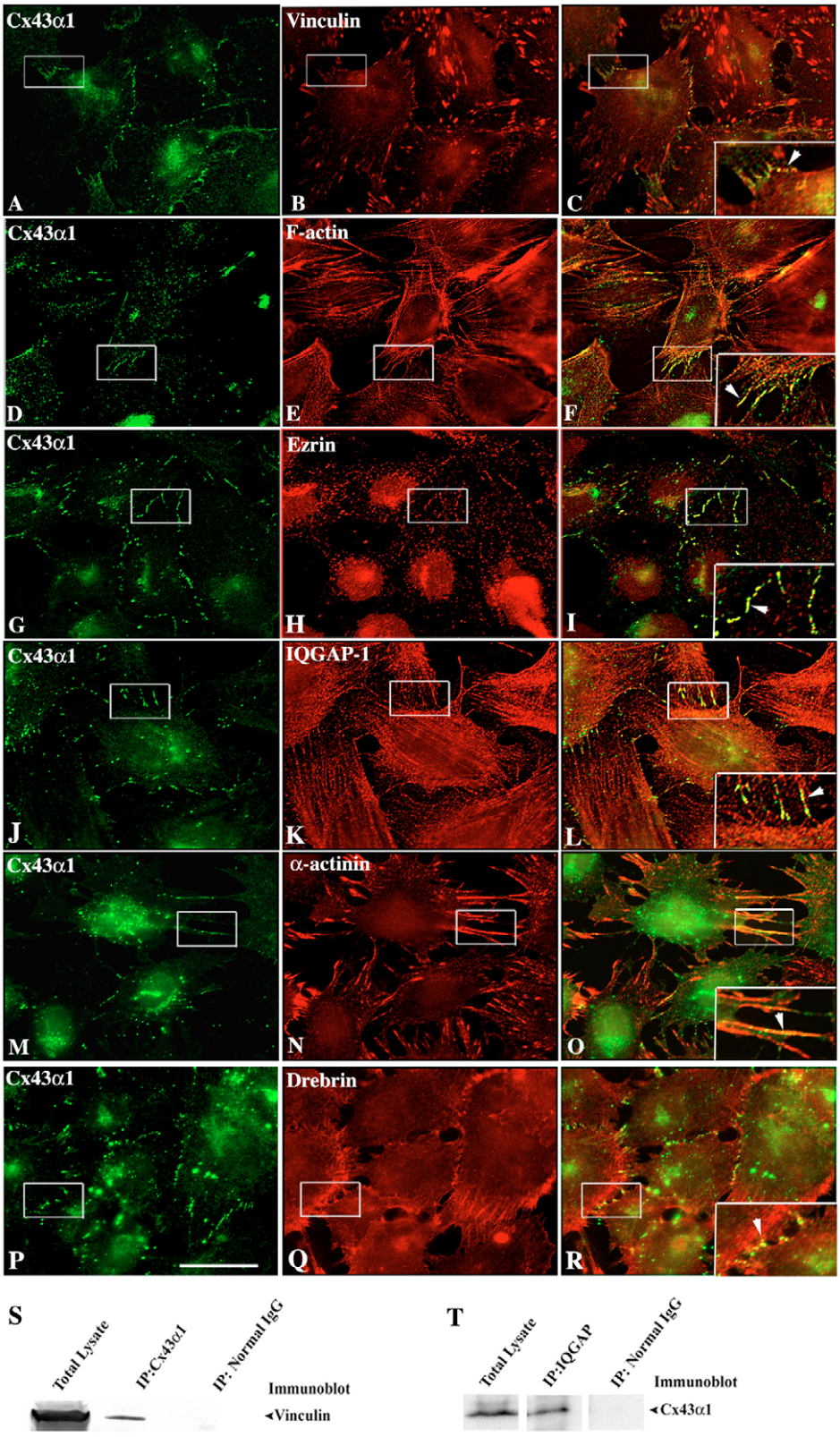


**Fig. 8. Cx43α1 colocalization with actin filaments and actin binding proteins.** CNCs were double immunostained for Cx43α1(green, **A**,**D**,**G**,**J**,**M**,**P**) and either vinculin (**B**), ezrin (**H**), IQGAP-1 (**K**), α-actinin (**N**) or drebrin (**Q**) in red. F-actin (**E**) was stained using rhodamine phalloidin. In the merged images (**C**,**F**,**I**,**L**,**O**,**R**), regions of Cx43α1 colocalization with actin or these various actin-associated proteins can be observed. These regions of colocalization were mostly found at areas of cell-cell contact and along cell processes (see white arrowhead in insets). Boxed regions are magnified twofold in the bottom insets. Scale bar: 50 μm. (**S**) NIH3T3 cell extracts were immunoprecipitated with a Cx43α1 antibody and western immunoblotted with a vinculin antibody. A band of the size expected for vinculin was observed in the Cx43α1 immunoprecipitate and in the total lysate. (**T**) NIH3T3 cell extracts were immunoprecipitated with an IQGAP-1 antibody and western immunoblotted with a Cx43α1 antibody. A band of the size expected for Cx43α1 was observed in the IQGAP-1 immunoprecipitate and in the total lysate.

performed co-immunoprecipitation and western immunoblotting using NIH3T3 cells, which, like neural crest cells, are highly motile and mesenchymal in cell morphology. NIH3T3 cell lysates were immunoprecipitated with a Cx43α1 antibody, followed by western immunoblotting with a vinculin antibody. Both proteins were co-immunoprecipitated (Fig. 8S). By contrast, similar analysis showed β1 integrin did not co-immunoprecipitate with Cx43α1, consistent with the fact that β1 integrin and Cx43α1 did not colocalize by immunohistochemistry (data not shown).

Using similar approaches, we also examined if Cx43α1 might interact with other actin-binding proteins. Using rhodamine phalloidin to delineate the actin cytoskeleton, we showed punctate

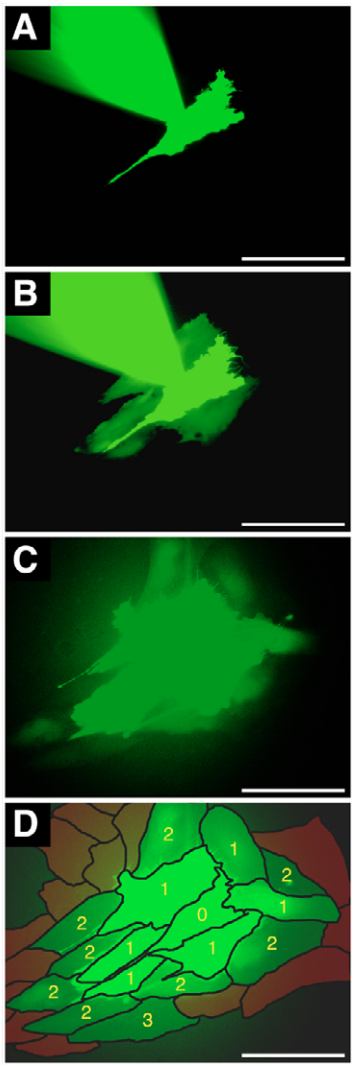


**Fig. 9. Quantitative analysis of dye coupling in CNCs.** (**A**) Intracellular microelectrode impalement and iontophoretic injection of 6-carboxyfluorescein in a CNC explant culture plated on 15 μg/ml fibronectin. (**B**) Extensive dye spread can be seen in the same explant after 2 minutes of iontophoretic dye injection. The microelectrode was removed at this 2-minute timepoint. (**C**) More extensive dye spread can be seen in the same explant after an additional 2 minutes to allow for continued spread of the injected dye. (**D**). To assess the precise extent of dye spread from the impaled cell (0) to primary (1), secondary (2) and tertiary neighbors (3), the dark-field fluorescence image in C was merged with the cell outlines obtained by tracing the DIC image of the same area. Shown in red are cells in the secondary or tertiary cell layers that did not contain the injected dye. Scale bars: 100 μm.

regions of Cx43α1 co-immunolocalization with actin filaments in CNCs (Fig. 8D-F). This was largely in extended cell processes encompassing regions of cell-cell contact. Double immunostaining further showed colocalization of Cx43α1 with several actin-binding proteins such as ezrin (Fig. 8G-I), IQGAP (Fig. 8J-L), α-actinin (Fig. 8M-O) and drebrin (Fig. 8P-R). Drebrin was recently identified as a new Cx43α1-binding partner (Butkevich et al., 2004). IQGAP (Fig. 8T), as well as α-actinin (data not shown) and drebrin (Butkevich et al., 2004), were all found to co-immunoprecipitate with Cx43α1. Overall, these findings suggest Cx43α1 is closely associated with multiprotein complexes containing vinculin and a variety of other actin-binding proteins.

### Gap junction communication unchanged with different fibronectin coating densities

To determine whether gap junction communication level might change with CNCs plated under different fibronectin density conditions, we carried out dye-coupling experiments. Previous studies of other cell types have reported an upregulation of gap junction communication with altered integrin-matrix interactions (Czyz et al., 2005; Lampe et al., 1998; Shanker et al., 2005). CNCs were impaled with microelectrodes and the gap junction permeable fluorescent tracer, carboxyfluorescein, was iontophoretically injected (Fig. 9). Upon impalement, the fluorescent dye quickly filled the impaled cell; over a period of 4 minutes, the injected dye rapidly spread to the surrounding cells, providing a direct visual display of gap junction mediated cell-cell communication (Fig. 9A-C). To quantitatively assess the extent of dye coupling, standard dye injection conditions were used (see Materials and methods), and the number of dye-filled cells was counted and expressed as a percentage of the total number of primary, secondary and tertiary neighbors (Fig. 9D; Table 2). Neural crest cells migrating on low concentration of fibronectin matrix were well coupled with dye spread to 78±8% primary, 45±15% secondary and 5.1±5.1% tertiary neighbors, respectively (Table 2). With fibronectin concentration elevated to 15 or 50 μg/ml, dye-coupling levels were not significantly changed (Table 2). These findings indicate no correlation between gap junction communication level and the fibronectin density.

## DISCUSSION

Our studies showed CNCs can migrate on a wide range of fibronectin density. They exhibited increased directionality, but decreased speed of cell locomotion as fibronectin density increased over a tenfold range. These observations contrast with cranial/trunk neural crest cells, which retain the same motile behavior over a wide range of fibronectin density (Strachan and Condic, 2003). The unique motile behavior of CNCs may facilitate their targeting to the heart, and perhaps underlie the sensitivity of this relatively small

**Table 2. Quantitative assessment of dye coupling**

| | Primary neighbors | | Secondary neighbors | | Tertiary neighbors | |
|---|---|---|---|---|---|---|
| Fibronectin coating* | Dye filled/total cells† | Dye filled‡ | Dye filled/total cells† | Dye filled‡ | Dye filled/total cells† | Dye filled‡ |
| 1 μg/ml (6) | 23/30 | 78±8% | 19/50 | 45±15% | 4/77 | 5.1±5% |
| 15 μg/ml (5) | 27/32 | 89±8% | 17/59 | 28±8% | 1/65 | 1.7±2% |
| 50 μg/ml (6) | 25/28 | 87±6% | 11/48 | 24±8% | 1/68 | 2.4±2% |

*Number in parenthesis indicates number of impalements.
†Sum of dye-filled cells/total cells from all impalements.
‡Mean±s.e.m. obtained from averaging the percentage of dye filled cells obtained with each impalement.

subpopulation of neural crest cells to developmental perturbations, whether genetically or environmentally induced. It is interesting that CNCs, when ablated, cannot be regenerated from the postotic hindbrain neural tube, nor from the mesencephalic or trunk neural crest cells (Kirby, 1989; Suzuki and Kirby, 1997). By contrast, hindbrain derived cephalic neural crest cells can regulate to reconstitute ablated neural crest cells (Baker et al., 1997; Saldivar et al., 1997; Scherson et al., 1993; Sechrist et al., 1995).

We showed that Sema3a can inhibit the adhesion and migration of CNCs on fibronectin. Sema3a significantly inhibited the extension and retraction of cell processes, and this was associated with an increase in the roundness of the cell. These effects are reminiscent of the growth cone collapse seen in neurons treated with semaphorins (Luo et al., 1993). They suggest semaphorins can regulate the deployment of CNCs by modulating motile cell behavior. Consistent with this, the *Sema3c* knockout mice exhibit persistent truncus arteriosus, an outflow septation defect similar to that seen in cardiac neural crest-ablated embryos (Feiner et al., 2001).

Our studies showed Cx43α1KO CNCs have poor motile function. They exhibited low directionality even on high fibronectin density, and this was associated with a reduction in vinculin immunostaining. By contrast, CMV43 CNCs show enhanced cell motility, with high directionality even at low fibronectin concentration. This was associated with increased vinculin immunostaining. These findings suggest alterations in cell surface linkage to the actin cytoskeleton may contribute to the changes in cell motility exhibited by the Cx43α1KO and CMV43 CNCs. Previous studies have shown that molecular changes affecting the strength of integrin-cytoskeletal linkages can alter the speed of cell locomotion (Lauffenburger and Horwitz, 1996; Schmidt et al., 1995). Although changes in the abundance of integrins also can affect cell motility, our cell surface biotinylation experiments indicated no change in cell surface β1 integrin expression level in the CMV43 CNCs.

Despite the poor motile function exhibited by Cx43α1KO CNCs, it is interesting to note that the Cx43α1KO CNCs actually showed increased protrusive activity. This was associated with a loss of polarized cell morphology. The latter is consistent with the reduced directionality of cell movement. Directional cell locomotion depends on the coordinated polarized assembly of new focal complexes at the leading edge of the cell and the disassembly of focal complexes at the cell rear (Huttenlocher et al., 1995; Lauffenburger and Horwitz, 1996). A defect in the release of cell processes was indicated by the effects of Sema3a on Cx43α1KO and CMV43 CNCs. Actin stress fibers play an important role in the retraction of the trailing edge of the cell and contraction of the cell body (Etienne-Manneville, 2004). In Cx43α1KO cells, the actin cytoskeleton showed a marked change, with stress fibers exhibiting a polygonal arrangement around the cell cortex, and with some stress fibers not anchored in focal adhesions. Cx43α1 was found to be closely associated with actin stress fibers at regions of cell-cell contact. Although Cx43α1 has not been shown to bind actin, Cx43α1 co-immunolocalized and co-immunoprecipitated with vinculin, and a number of other actin-binding proteins, including IQGAP-1, drebrin and α-actinin. Together with previous reports showing binding of Cx43α1 with ZO-1, and the close association of Cx43α1 with β-catenin and α-catenin (Giepmans and Moolenaar, 1998; Ai et al., 2000; Govindarajan et al., 2002; Wei et al., 2005; Wu et al., 2003), an important role is indicated for Cx43α1 in the dynamic regulation of the actin cytoskeleton.

Our studies showed no correlation between the level of dye coupling and changes in motile cell behavior. This is similar to the results of our earlier studies examining motile cell behavior and dye coupling levels in CNCs derived from a variety of different transgenic and knockout mouse models (Xu et al., 2001). Overall, these findings do not support a role for cell-cell communication via gap junction channels in modulating cell motility. However, we cannot exclude a role for gap junction mediated coupling, and a recent study reported that migrating neural crest cells maintain short and long distance cell-cell contacts with other migrating crest cells (Teddy and Kulesa, 2004). Based on our present studies, we suggest Cx43α1 may serve a novel signaling function that entails crosstalk with cell signaling pathways that regulate polarized cell morphology. Overall, these findings provides a framework for future investigations into the dynamic regulation of the actin cytoskeleton and motile cell behavior by Cx43α1.

We thank Dr Tom Borg for kindly providing β1 integrin function blocking antibody, Dr Elliot Hertzberg for providing Cx43α1 antibody and Dr Diana Walker for helpful discussions. This work was supported by funding from the Division of Intramural Research of NHLBI/NIH.

**Supplementary material**

Supplementary material for this article is available at
http://dev.biologists.org/cgi/content/full/133/18/3629/DC1

**References**

**Ai, Z., Fischer, A., Spray, D. C., Brown, A. M. and Fishman, G. I.** (2000). Wnt-1 regulation of connexin43 in cardiac myocytes. *J. Clin. Invest.* **105**, 161-171.

**Alfandari, D., Cousin, H., Gaultier, A., Hoffstrom, B. G. and DeSimone, D. W.** (2003). Integrin alpha5beta1 supports the migration of Xenopus cranial neural crest on fibronectin. *Dev. Biol.* **260**, 449-464.

**Baker, C. V., Bronner-Fraser, M., Le Douarin, N. M. and Teillet, M. A.** (1997). Early- and late-migrating cranial neural crest cell populations have equivalent developmental potential in vivo. *Development* **124**, 3077-3087.

**Brown, C. B., Feiner, L., Lu, M. M., Li, J., Ma, X., Webber, A. L., Jia, L., Raper, J. A. and Epstein, J. A.** (2001). PlexinA2 and semaphorin signaling during cardiac neural crest development. *Development* **128**, 3071-3080.

**Butkevich, E., Hulsmann, S., Wenzel, D., Shirao, T., Duden, R. and Majoul, I.** (2004). Drebrin is a novel connexin-43 binding partner that links gap junctions to the submembrane cytoskeleton. *Curr. Biol.* **14**, 650-658.

**Czyz, J., Guan, K., Zeng, Q. and Wobus, A. M.** (2005). Loss of beta1 integrin function results in upregulation of connexin expression in embryonic stem cell-derived cardiomyocytes. *Int. J. Dev. Biol.* **49**, 33-41.

**De Bellard, M. E., Ching, W., Gossler, A. and Bronner-Fraser, M.** (2002). Disruption of segmental neural crest migration and ephrin expression in delta-1 null mice. *Dev. Biol.* **249**, 121-130.

**Delannet, M., Martin, F., Bossy, B., Cheresh, D. A., Reichardt, L. F. and Duband, J. L.** (1994). Specific roles of the alpha V beta 1, alpha V beta 3 and alpha V beta 5 integrins in avian neural crest cell adhesion and migration on vitronectin. *Development* **120**, 2687-2702.

**Etienne-Manneville, S.** (2004). Actin and microtubules in cell motility: which one is in control? *Traffic* **5**, 470-477.

**Feiner, L., Webber, A. L., Brown, C. B., Lu, M. M., Jia, L., Feinstein, P., Mombaerts, P., Epstein, J. A. and Raper, J. A.** (2001). Targeted disruption of semaphorin 3C leads to persistent truncus arteriosus and aortic arch interruption. *Development* **128**, 3061-3070.

**Giepmans, B. N. and Moolenaar, W. H.** (1998). The gap junction protein connexin43 interacts with the second PDZ domain of the zona occludens-1 protein. *Curr. Biol.* **8**, 931-934.

**Govindarajan, R., Zhao, S., Song, X. H., Guo, R. J., Wheelock, M., Johnson, K. R. and Mehta, P. P.** (2002). Impaired trafficking of connexins in androgen-independent human prostate cancer cell lines and its mitigation by alpha-catenin. *J. Biol. Chem.* **277**, 50087-50097.

**Gullberg, D., Terracio, L., Borg, T. K. and Rubin, K.** (1989). Identification of integrin-like matrix receptors with affinity for interstitial collagens. *J. Biol. Chem.* **264**, 12686-12694.

**Huang, G. Y., Cooper, E. S., Waldo, K., Kirby, M. L., Gilula, N. B. and Lo, C. W.** (1998a). Gap junction-mediated cell-cell communication modulates mouse neural crest migration. *J. Cell Biol.* **143**, 1725-1734.

**Huang, G. Y., Wessels, A., Smith, B. R., Linask, K. K., Ewart, J. L. and Lo, C. W.** (1998b). Alteration in connexin 43 gap junction gene dosage impairs conotruncal heart development. *Dev. Biol.* **198**, 32-44.

**Huttenlocher, A., Sandborg, R. R. and Horwitz, A. F.** (1995). Adhesion in cell migration. *Curr. Opin. Cell Biol.* **7**, 697-706.

**Kirby, M. L.** (1989). Plasticity and predetermination of mesencephalic and trunk neural crest transplanted into the region of the cardiac neural crest. *Dev. Biol.* **134**, 402-412.

**Kirby, M. L. and Waldo, K. L.** (1995). Neural crest and cardiovascular patterning. *Circ. Res.* **77**, 211-215.
**Kirby, M. L., Gale, T. F. and Stewart, D. E.** (1983). Neural crest cells contribute to normal aorticopulmonary septation. *Science* **220**, 1059-1061.
**Lampe, P. D., Nguyen, B. P., Gil, S., Usui, M., Olerud, J., Takada, Y. and Carter, W. G.** (1998). Cellular interaction of integrin alpha3beta1 with laminin 5 promotes gap junctional communication. *J. Cell Biol.* **143**, 1735-1747.
**Lauffenburger, D. A. and Horwitz, A. F.** (1996). Cell migration: a physically integrated molecular process. *Cell* **84**, 359-369.
**Lee, Y. M., Osumi-Yamashita, N., Ninomiya, Y., Moon, C. K., Eriksson, U. and Eto, K.** (1995). Retinoic acid stage-dependently alters the migration pattern and identity of hindbrain neural crest cells. *Development* **121**, 825-837.
**Li, W. E., Waldo, K., Linask, K. L., Chen, T., Wessels, A., Parmacek, M. S., Kirby, M. L. and Lo, C. W.** (2002). An essential role for connexin43 gap junctions in mouse coronary artery development. *Development* **129**, 2031-2042.
**Lo, C. W., Waldo, K. L. and Kirby, M. L.** (1999). Gap junction communication and the modulation of cardiac neural crest cells. *Trends Cardiovasc. Med.* **9**, 63-69.
**Lumsden, A., Sprawson, N. and Graham, A.** (1991). Segmental origin and migration of neural crest cells in the hindbrain region of the chick embryo. *Development* **113**, 1281-1291.
**Luo, Y., Raible, D. and Raper, J. A.** (1993). Collapsin: a protein in brain that induces the collapse and paralysis of neuronal growth cones. *Cell* **75**, 217-227.
**Moiseiwitsch, J. R. and Lauder, J. M.** (1995). Serotonin regulates mouse cranial neural crest migration. *Proc. Natl. Acad. Sci. USA* **92**, 7182-7186.
**Monier-Gavelle, F. and Duband, J. L.** (1997). Cross talk between adhesion molecules: control of N-cadherin activity by intracellular signals elicited by beta1 and beta3 integrins in migrating neural crest cells. *J. Cell Biol.* **137**, 1663-1681.
**Osborne, N. J., Begbie, J., Chilton, J. K., Schmidt, H. and Eickholt, B. J.** (2005). Semaphorin/neuropilin signaling influences the positioning of migratory neural crest cells within the hindbrain region of the chick. *Dev. Dyn.* **232**, 939-949.
**Pasterkamp, R. J., Peschon, J. J., Spriggs, M. K. and Kolodkin, A. L.** (2003). Semaphorin 7A promotes axon outgrowth through integrins and MAPKs. *Nature* **424**, 398-405.
**Reaume, A. G., de Sousa, P. A., Kulkarni, S., Langille, B. L., Zhu, D., Davies, T. C., Juneja, S. C., Kidder, G. M. and Rossant, J.** (1995). Cardiac malformation in neonatal mice lacking connexin43. *Science* **267**, 1831-1834.
**Saldivar, J. R., Sechrist, J. W., Krull, C. E., Ruffins, S. and Bronner-Fraser, M.** (1997). Dorsal hindbrain ablation results in rerouting of neural crest migration and changes in gene expression, but normal hyoid development. *Development* **124**, 2729-2739.
**Scherson, T., Serbedzija, G., Fraser, S. and Bronner-Fraser, M.** (1993). Regulative capacity of the cranial neural tube to form neural crest. *Development* **118**, 1049-1062.
**Schmidt, C. E., Dai, J., Lauffenburger, D. A., Sheetz, M. P. and Horwitz, A. F.** (1995). Integrin-cytoskeletal interactions in neuronal growth cones. *J. Neurosci.* **15**, 3400-3407.
**Sechrist, J., Nieto, M. A., Zamanian, R. T. and Bronner-Fraser, M.** (1995). Regulative response of the cranial neural tube after neural fold ablation: spatiotemporal nature of neural crest regeneration and up-regulation of Slug. *Development* **121**, 4103-4115.
**Serini, G., Valdembri, D., Zanivan, S., Morterra, G., Burkhardt, C., Caccavari, F., Zammataro, L., Primo, L., Tamagnone, L., Logan, M. et al.** (2003). Class 3 semaphorins control vascular morphogenesis by inhibiting integrin function. *Nature* **424**, 391-397.
**Shanker, A. J., Yamada, K., Green, K. G., Yamada, K. A. and Saffitz, J. E.** (2005). Matrix protein-specific regulation of Cx43 expression in cardiac myocytes subjected to mechanical load. *Circ. Res.* **96**, 558-566.
**Southard-Smith, E. M., Kos, L. and Pavan, W. J.** (1998). Sox10 mutation disrupts neural crest development in Dom Hirschsprung mouse model. *Nat. Genet.* **18**, 60-64.
**Stites, J., Wessels, D., Uhl, A., Egelhoff, T., Shutt, D. and Soll, D. R.** (1998). Phosphorylation of the Dictyostelium myosin II heavy chain is necessary for maintaining cellular polarity and suppressing turning during chemotaxis. *Cell Motil. Cytoskeleton* **39**, 31-51.
**Strachan, L. R. and Condic, M. L.** (2003). Neural crest motility and integrin regulation are distinct in cranial and trunk populations. *Dev. Biol.* **259**, 288-302.
**Sullivan, R. and Lo, C. W.** (1995). Expression of a connexin 43/beta-galactosidase fusion protein inhibits gap junctional communication in NIH3T3 cells. *J. Cell Biol.* **130**, 419-429.
**Suzuki, H. R. and Kirby, M. L.** (1997). Absence of neural crest cell regeneration from the postotic neural tube. *Dev. Biol.* **184**, 222-233.
**Teddy, J. M. and Kulesa, P. M.** (2004). In vivo evidence for short- and long-range cell communication in cranial neural crest cells. *Development* **131**, 6141-6151.
**Waldo, K., Zdanowicz, M., Burch, J., Kumiski, D. H., Stadt, H. A., Godt, R. E., Creazzo, T. L. and Kirby, M. L.** (1999). A novel role for cardiac neural crest in heart development. *J. Clin. Invest.* **103**, 1499-1507.
**Wei, C. J., Francis, R., Xu, X. and Lo, C. W.** (2005). Connexin43 associated with an N-cadherin containing multi-protein complex is required for gap junction formation in NIH3T3 cells. *J. Biol. Chem.* **280**, 19925-19936.
**Wu, J. C., Tsai, R. Y. and Chung, T. H.** (2003). Role of catenins in the development of gap junctions in rat cardiomyocytes. *J. Cell Biochem.* **88**, 823-835.
**Xu, X., Li, W. E., Huang, G. Y., Meyer, R., Chen, T., Luo, Y., Thomas, M. P., Radice, G. L. and Lo, C. W.** (2001). Modulation of mouse neural crest cell motility by N-cadherin and connexin 43 gap junctions. *J. Cell Biol.* **154**, 217-230.